CHEMISTRY OF MATERIALS
Cite This: Chem. Mater. 2018, 30, 6431−6439
Article
pubs.acs.org/cm

Nitrogen-Doped Carbon Nanomaterials as Highly Active and Specific Peroxidase Mimics

Yihui Hu,[†,⊥,#] Xuejiao J. Gao,[§,#] Yunyao Zhu,[†] Faheem Muhammad,[†] Shihua Tan,[‡] Wen Cao,[†] Shichao Lin,[†] Zhong Jin,[∥] Xingfa Gao,[*,§] and Hui Wei[*,†,¶]

[†]Department of Biomedical Engineering, College of Engineering and Applied Sciences, Collaborative Innovation Center of Chemistry for Life Sciences, Nanjing National Laboratory of Microstructures, Nanjing University, Nanjing, Jiangsu 210093, China

[§]College of Chemistry and Chemical Engineering, Jiangxi Normal University, Nanchang 330022, China

[‡]Institute of Mathematics and Physics, Central South University of Forestry & Technology, Changsha 410004, China

[∥]Key Laboratory of Mesoscopic Chemistry of MOE, School of Chemistry and Chemical Engineering, Nanjing University, Nanjing, Jiangsu 210023, China

[¶]State Key Laboratory of Analytical Chemistry for Life Science, School of Chemistry and Chemical Engineering, Nanjing University, Nanjing, Jiangsu 210093, China

[⊥]Key Laboratory of Drug Quality Control and Pharmacovigilance, China Pharmaceutical University, Ministry of Education, Nanjing 210009, China

Supporting Information

ABSTRACT: Nanozymes, the enzyme-mimicking nanomaterials, have been developed to overcome the low stability and high cost of natural enzymes. Unlike highly active and specific enzymes, however, the catalytic activities of nanozymes are moderate and lack specificity. To address these issues, herein we demonstrated an effective and general strategy to specifically enhance the peroxidase-mimicking activities of carbon nanozymes. By doping heteroatom nitrogen (N) into reduced graphene oxide (rGO) and mesoporous carbon (MC), their peroxidase-mimicking activities were enhanced by over 100- and 60-fold, respectively. Moreover, N-doping did not significantly affect the oxidase-, superoxide dismutase (SOD)-, or catalase-mimicking activities of rGO and MC, demonstrating a specific enhancement of the peroxidase-mimicking activities. To understand the origin of the specific enhancement, we performed density functional theory calculations to examine the catalytic reaction mechanisms responsible for the peroxidase-, catalase-, oxidase-, and SOD-mimicking activities of N-doped rGO (N-rGO). We revealed that N-rGO selectively activated H_2O_2 rather than O_2 and $^{\bullet}O_2^-$ by forming and stabilizing radical oxygen species adjacent to the N sites of N-rGO. The radical oxygen species then oxidized peroxidase substrates, endowing N-rGO with peroxidase-mimicking activity. This study will aid in the rational design of highly active and specific peroxidase mimics and help elucidate the catalytic mechanisms of nanozymes.

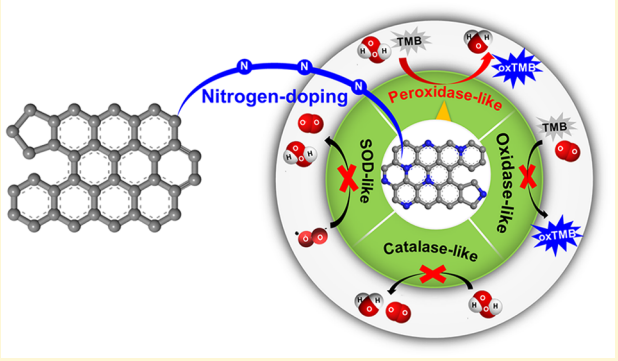

INTRODUCTION

Nanomaterials-based enzyme mimics (called nanozymes) have received great attention due to their high stability, low cost, and multifunctionalities.[1] Though a variety of nanomaterials (such as metal, metal oxides, and carbon nanomaterials) have been studied as enzyme mimics during recent decades, the catalytic activities of nanozymes developed to date are still moderate and lack specificity.[1−26] These shortcomings have limited their broad application in areas such as biosensing, bioimaging, and nanomedicine.[27] To overcome these shortcomings, on one hand, numerous strategies have been developed to improve the activities of nanozymes by modulating their sizes, morphologies, or compositions.[1,28−30] For example, multiple enzyme-mimicking activities of carbon nanozymes were enhanced by heteroatom nitrogen (N)-doping.[31,32] However, the mechanisms underlying the activity enhancement of carbon nanozymes by N-doping have yet to be elucidated, which, if available, would guide to design highly active nanozymes. On the other hand, the specificity of nanozyme-catalyzed reactions has largely not been fulfilled. Most nanozymes possess multiple enzyme-mimicking activities.[33−35] For example, both fullerenes and carbon nanodots were reported to mimic the activities of peroxidase and superoxide dismutase (SOD).[32,36−39] Recently, Liu et al. attempted to address the issue of nanozymes' specificity. They showed that the substrate specificity of peroxidase-like

Received: June 27, 2018
Revised: August 19, 2018
Published: August 20, 2018

DOI: 10.1021/acs.chemmater.8b02726
Chem. Mater. 2018, 30, 6431−6439

nanozymes was enhanced by growing molecularly imprinted polymers on the surfaces of the nanomaterials.[3] However, the intrinsic specificity of nanozymes has yet to be addressed, which, if achieved, would truly imitate one of the characteristics of enzyme catalysis.

To address these issues, herein we reported an unexpected finding that N-doping into reduced graphene oxide (rGO) not only boosts its peroxidase-mimicking activities by 2 orders of magnitude but also achieves exceptional specificity toward peroxidase-mimicking activity and not other closely related enzymatic reactions (Figure 1). To understand the origin of

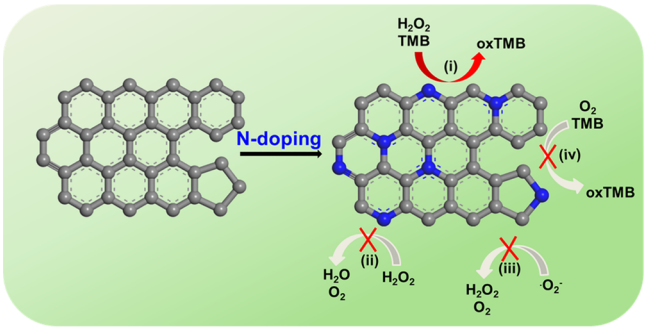

Figure 1. N-rGO exhibits specifically enhanced peroxidase-mimicking activity (i) but negligible catalase-, SOD-, and oxidase-mimicking activities (ii, iii, and iv, respectively). TMB: 3,3′,5,5′-tetramethylbenzidine dihydrochloride hydrate; oxTMB: oxidized TMB.

the highly active and specific peroxidase-mimicking activity of N-doped rGO (N-rGO), we performed density functional theory (DFT) calculations. We revealed that N-rGO selectively activates H_2O_2 rather than O_2 and $^{\bullet}O_2^-$ by forming and stabilizing radical oxygen species adjacent to the N sites of N-rGO. The radical oxygen species then oxidize peroxidase substrates, endowing N-rGO with specific peroxidase-mimicking activity. Moreover, we demonstrated that N-doping is a general strategy for specifically enhancing the peroxidase-mimicking activities of carbon nanomaterials.

EXPERIMENTAL SECTION

Chemicals and Materials. Graphene oxide (GO) was obtained from Nanjing XFNANO Co. Ltd. and had diameters of 0.5−5 μm and thicknesses of 0.8−1.2 nm. 5,5-Dimethyl-1-pyrroline *N*-oxide (DMPO) was obtained from J&K Chemicals (Shanghai, China). Xanthine, xanthine oxidase, hydrogen peroxide (30%), and hydroethidine were purchased from Sigma−Aldrich. Urea, iron(II) sulfate heptahydrate, hydrofluoric acid, and acetic acid were purchased from Sinopharm Chemical Reagent Co., Ltd. (Shanghai, China). 3,3′,5,5′-Tetramethylbenzidine dihydrochloride hydrate (TMB), hexadecyltrimethylammonium bromide (CTAB), tetraethyl orthosilicate (TEOS), and *p*-phthalic acid (PTA) were obtained from Aladdin (Shanghai, China). Cyanamide was purchased from Alfa Aesar. Sodium dihydrogen phosphate dihydrate, disodium hydrogen phosphate dodecahydrate, and anhydrous sodium acetate were purchased from Nanjing Chemical Co. (Nanjing, China). Other chemicals were of at least analytical reagent grade and were used as received. All aqueous solutions were prepared with deionized water (18.2 MΩ·cm, Millipore).

Instrumentation. Transmission electron microscopy (TEM) imaging was performed on a Tecnai F20 microscope at an acceleration voltage of 200 kV (FEI, USA). Scanning electron microscopy (SEM) images were recorded on a Zeiss Ultra 55 microscope (Zeiss, Germany). X-ray photoelectron spectroscopy (XPS) spectra were collected by a PHI 5000 VersaProbe XPS microscope (UlVAC-PHI, Japan). Electron paramagnetic resonance (EPR) measurements were carried out on a Bruker EMX-10/12 spectrometer (Bruker, Germany). UV−visible absorption spectra were collected on a UV−visible spectrophotometer (Beijing Purkinje General Instrument Co., Ltd., China), and fluorescence spectra were measured on a Hitachi F-4600 fluorescence spectrophotometer (Hitachi, Japan).

Synthesis of rGO and N-rGO. rGO was obtained by annealing GO under an Ar atmosphere for 1 h in a tubular furnace at 600 °C with a heating rate of 3 °C/min, followed by further annealing for 3 h at 900 °C with a heating rate of 5 °C/min. After cooling to room temperature, the rGO samples were ground.

N-rGO was obtained using two methods, depending on the nitrogen source, as follows:

(1) Urea as a nitrogen source for N-rGO.[40] First, GO (50 mg) was dispersed in ethanol (25 mL) by sonicating the mixture for 10 min. Then, different amounts of urea were added into the mixture and thoroughly mixed by sonicating the mixture for another 60 min. The mixture was then transferred into a 100 mL beaker, stirred, and heated at 80 °C to dryness. The dried samples were heated under an Ar flow for 1 h at 600 °C with a heating rate of 3 °C/min. Next, the temperature was increased to 700, 800, 900, or 1000 °C at a heating rate of 5 °C/min and maintained at that temperature for 3 h to afford N-rGO (samples are denoted N-rGO-1, N-rGO-2, N-rGO-3, N-rGO-4, and N-rGO-5, see Figure S2). After cooling to room temperature, the N-rGO samples were ground.

(2) Ammonia as a nitrogen source for N-rGO.[41] First, GO (30 mg) was loaded in a tube furnace under a flow of 5% NH_3 in Ar. The GO was then annealed for 2 h after reaching the desired temperature (600, 800, or 1000 °C) with a heating rate of 3 °C/min (samples are denoted N-rGO-6, N-rGO-7, and N-rGO-8, see Figure S2). After cooling to room temperature, the N-rGO samples were ground.

Synthesis of Mesoporous Carbon (MC) and N-Mesoporous Carbon (N-MC). MC and N-MC were synthesized using a template-mediated strategy.

Synthesis of the Mesoporous Silica Template.[42] In a typical procedure, CTAB (162.5 mg, 0.09 equiv) was dissolved in 78.9 mL of aqueous solution containing ethanol (25.4 mL, 115 equiv) and concentrated aqueous NH_3 (1 mL, 25 wt %, 2.96 equiv). Then, the mixture was heated to 35 °C, and TEOS (1 mL, 1 equiv) was rapidly added with vigorous stirring. After stirring at 35 °C for 24 h, the resulting white product was collected by centrifugation at 4000 rpm for 10 min and washed three times with ethanol. The CTAB template was then removed by calcining the sample at 550 °C for 5 h.

Synthesis of N-MC.[43] Oxalic acid (6 mg), a polymerization catalyst, was dissolved in furfuryl alcohol (1 mL), followed by the addition of cyanimide (100 mg) with sonication. The obtained solution was then infiltrated into the mesoporous silica pores by a wetness impregnation technique at room temperature.[44] Polymerization was achieved by heating the sample at 80 °C for 12 h, and then the composite was calcined under an Ar flow using the following program: (1) 150 °C for 2 h; (2) heating to 650 °C at 2 °C/min and holding at this temperature for 5 h. The silica template was subsequently removed by treating the composite with 10% HF for 24 h. The black powder was centrifuged at 8000 rpm for 5 min and thoroughly washed with water and ethanol. Finally, the N-MC was dried at 60 °C in vacuum oven overnight.

Synthesis of MC. The same method was used as for the synthesis of N-MC, without the addition of cyanimide.

Peroxidase-Mimicking Activity Measurements. The carbon-based nanozyme (1 mg/mL, 5 μL) was added into NaOAc−HOAc buffer (100 mM, pH 4.0) containing H_2O_2 (10 M, 1 μL) and TMB (25 mM, 10 μL). The final volume of the mixture was adjusted to 500 μL with NaOAc−HOAc buffer (100 mM, pH 4.0). Then, a portion (200 μL) of the mixture was used for UV−visible spectroscopy measurements at an absorbance of 652 nm for the time-course experiment.

Oxidase-Mimicking Activity Measurements. The carbon-based nanozyme (1 mg/mL, 5 μL) was added into NaOAc−HOAc buffer (100 mM, pH 4.0) containing TMB (25 mM, 10 μL). The final volume of the mixture was adjusted to 500 μL with NaOAc−HOAc

DOI: 10.1021/acs.chemmater.8b02726
Chem. Mater. 2018, 30, 6431−6439

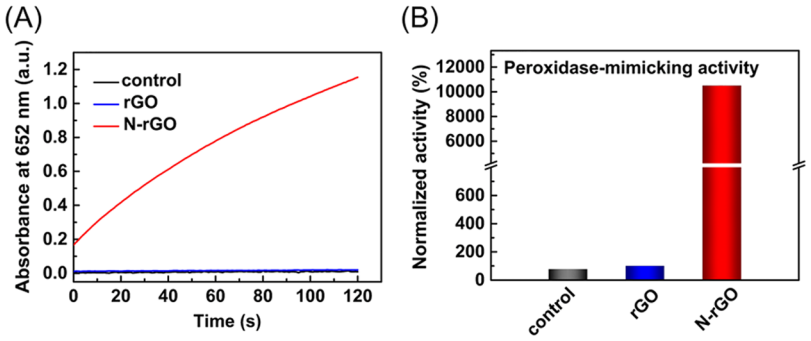

Figure 2. (A) Kinetic curves of A_{652} for monitoring the catalytic oxidation of 500 μM TMB (100 mM NaOAc−HOAc buffer, pH 4.0) with 20 mM H_2O_2 in the presence of 10 μg/mL rGO or 10 μg/mL N-rGO-5. (B) Normalized peroxidase-mimicking activities of rGO and N-rGO-5.

buffer (100 mM, pH 4.0). Then, a portion (200 μL) of the mixture was used for UV−visible spectroscopy measurements at an absorbance of 652 nm in the time-course experiment.

Catalase-Mimicking Activity Measurements. In a typical procedure, carbon-based nanozyme (1 mg/mL, 4 μL) was added into phosphate-buffered saline buffer (0.10 M, pH 7.0, 196 μL) containing H_2O_2 (1 M). Then, the reactor was quickly sealed. The O_2 pressure was measured with a pressure gauge after 10 min.

SOD-Mimicking Activity Measurements. Xanthine was catalytically oxidized with xanthine oxidase to produce $^{\bullet}O_2^-$. Hydroethidine, an $^{\bullet}O_2^-$ specific fluorescence probe, was used to assess the amount of $^{\bullet}O_2^-$. In a typical procedure, carbon-based nanozyme (1 mg/mL, 5 μL) was added into NaOAc−HOAc buffer (5 mM, pH 4.0, 485 μL) containing xanthine (0.6 mM) and xanthine oxidase (40 mU). After incubation for 10 min, hydroethidine (10 mg/mL, 10 μL) was added and allowed to react for 30 min. The fluorescence was then measured with an excitation wavelength of 510 nm.

Monitoring $^{\bullet}$OH Elimination by the Nanozymes by Fluorescence. H_2O_2 (50 mM), PTA (0.5 mM), and different amounts of carbon-based nanozyme were added into NaOAc−HOAc buffer (100 mM, pH 4.0) and reacted for 30 min under UV irradiation with 365 nm. Then, the mixture was centrifuged at 10 000 rpm for 2 min, and the supernatant was used for fluorescence measurements with an excitation wavelength of 315 nm.

Monitoring $^{\bullet}$OH Elimination by the Nanozymes by EPR Spectroscopy. H_2O_2 (100 mM), DMPO (100 mM), iron sulfate heptahydrate (0.2 mM), and carbon-based nanozymes (30 μg/mL) were added into a NaOAc−HOAc buffer (100 mM, pH 4.0) and mixed thoroughly. Then, the mixture was transferred into a capillary tube for EPR measurements.

Structural Models and Computational Methods. The N atoms in N-rGO have four main structural configurations: pyridinic N, pyrrolic N, graphitic N (i.e., quaternary nitrogen), and oxidic N (Figure S1A).[45] Among them, graphitic N has been verified as the catalytically active site for various redox reactions, such as oxygen reduction reaction[46] and water oxidation.[47] Because the enzyme-mimicking activities studied here are redox reactions involving similar oxygen species (Figure 1), the graphitic N should be the most important active site, deserving of special attention. Therefore, our computational study focused on the graphitic N of N-rGO.

We used the small-sized molecules pyrene and coronene and two-dimensional, size-infinite graphene as the three different models of rGO, that is, N-doped pyrene (N-pyrene), N-doped coronene (N-coronene), and N-doped graphene (N-graphene), respectively (Figure S1B−1D). For the N-pyrene and N-coronene models, one of the peripheral sp^2 C atoms was saturated by the addition of an H atom to keep the closed-shell singlet in the ground state. In these models, the oxygen-containing groups, which were experimentally found in rGO and N-rGO, were not considered because the present study focused on the effect of N-doping in the main structure, i.e., the sp^2 domain, of rGO. The role of oxygen functionalities in GO in the enzyme-mimicking activities has been studied previously.[19,48]

For the N-pyrene and N-coronene models, the geometries were optimized using the B3LYP functional[49] with the 6-31G(d,p) basis set. The solvent effect of water was considered using the polarizable continuum model.[50] The system temperature was set as 298.15 K. The frequency analyses for all structures were performed at the same level of theory to obtain Gibbs free energies. The frequency calculations confirmed that each energy minimum has no imaginary frequencies and that each transition state has only one imaginary frequency. All these calculations were performed using the Gaussian 09 package.[51] Similar methods have been successfully applied to study the chemical reactions of carbon clusters, including polycyclic hydrocarbons and fullerenes.[48,51]

With the periodic graphene and N-graphene models, the calculations were performed using the Vienna ab initio Simulation Package (VASP).[52] A (4 × 4) graphene supercell with 32 C atoms was taken as the graphene model, and the same graphene supercell with one C atom substituted by one N was used as the N-graphene model. The Perdew−Burke−Ernzerhof functional[53] was used for geometry optimization and energy calculations in a plane-wave basis set with an energy cutoff of 500 eV and Gaussian smearing of 0.05 eV. A vacuum height of 15 Å was set in the vertical directions to avoid the interaction between periodic images. The Brillouin zones were sampled with the (3 × 3 × 1) Monkhorst−Pack[54] mesh k-point grids. The convergence criteria of the electronic energy and forces were set to 10^{-5} eV and 0.01 eV/Å, respectively.

RESULTS AND DISCUSSION

Enhancing the Peroxidase-Mimicking Activity of rGO by N-Doping. First, we studied the enhanced peroxidase-mimicking activity of rGO after N-doping. rGO was chosen as a representative nanozyme due to its robust activity and biocompatibility. After optimization of the synthetic conditions (Figure S2), N-rGO-5 with the highest peroxidase-like activity was obtained, which was further investigated and compared with rGO in subsequent studies. The peroxidase-like activities of rGO and N-rGO-5 were evaluated by monitoring TMB oxidation with H_2O_2 in the presence of the nanozymes. Surprisingly, the reaction solution containing N-rGO showed a much more intense blue color than that containing rGO (Figure S6). This clearly indicated that the peroxidase-like activity of rGO was remarkably enhanced after N-doping. We quantitatively studied the catalytic activity of N-rGO-5 by monitoring the absorbance of oxidized TMB (oxTMB) at 652 nm (A_{652}; Figure 2A), which revealed that N-rGO-5 exhibited more than 2 orders of magnitude higher activity than pristine rGO (a 105-fold enhancement; Figure 2B).

Kinetics Studies. To understand the enhanced peroxidase-mimicking activity of N-rGO-5, the steady-state kinetics of the rGO and N-rGO-5 nanozymes were investigated (Figures S10 and S11). With increasing substrate concentration, the catalytic

DOI: 10.1021/acs.chemmater.8b02726
Chem. Mater. 2018, 30, 6431−6439

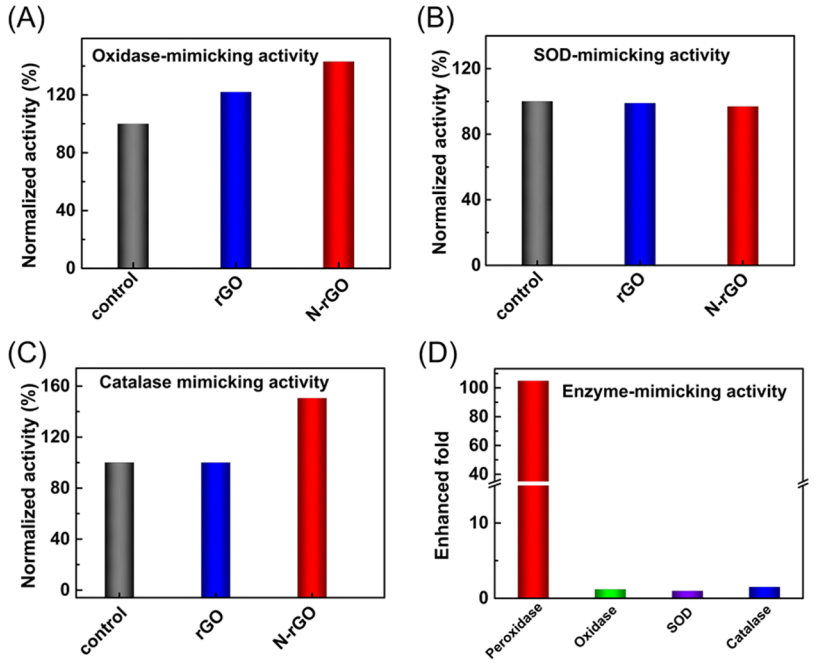

Figure 3. Specifically enhancing the peroxidase-mimicking activity of rGO by N-doping. (A) Oxidase-, (B) SOD-, and (C) catalase-mimicking activities of rGO and N-rGO-5. Control sample did not contain any nanozymes. (D) Enhancement of the enzyme-mimicking activities of N-rGO-5 relative to those of rGO.

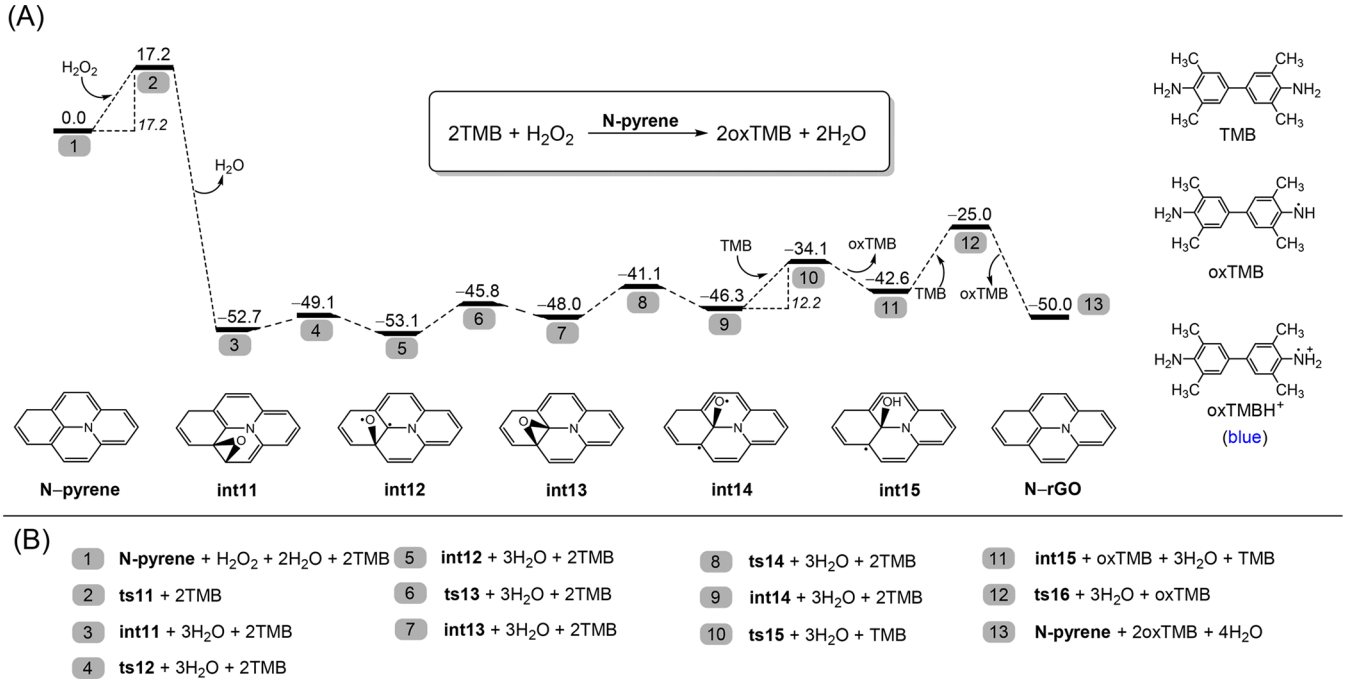

Figure 4. Calculated reaction energy profiles corresponding to the prominent peroxidase-mimicking activity of N-pyrene, i.e., the small-sized model of N-rGO. (A) Reaction free energy profiles for the catalytic cycle through which TBM is oxidized to oxTMB by H_2O_2 with N-pyrene as the catalyst (energy in kcal/mol). (B) Chemical constituents for the stationary points shown in panel A.

speed increased gradually and reached a plateau, which suggested that the nanozyme-catalyzed reactions obeyed Michaelis−Menten kinetics. As shown in Table S1, the K_m value of N-rGO-5 for H_2O_2 was lower than that of rGO, indicating that N-rGO-5 has a higher affinity for H_2O_2 than rGO. However, the K_m value of N-rGO-5 for TMB was higher than that of rGO, suggesting rGO has a higher affinity for TMB than N-rGO-5. These differences were consistent with the DFT calculation study (vide infra), which showed that the activation of H_2O_2 is the rate-determining step for the catalysis. Moreover, the V_{max} values of N-rGO-5 for both H_2O_2 and TMB were much higher than those of rGO, further confirming that N-doping improved the peroxidase-mimicking activity of rGO.

Specifically Mimicking Peroxidase with N-rGO. We then studied the other closely related redox enzyme-mimicking

DOI: 10.1021/acs.chemmater.8b02726
Chem. Mater. 2018, 30, 6431−6439

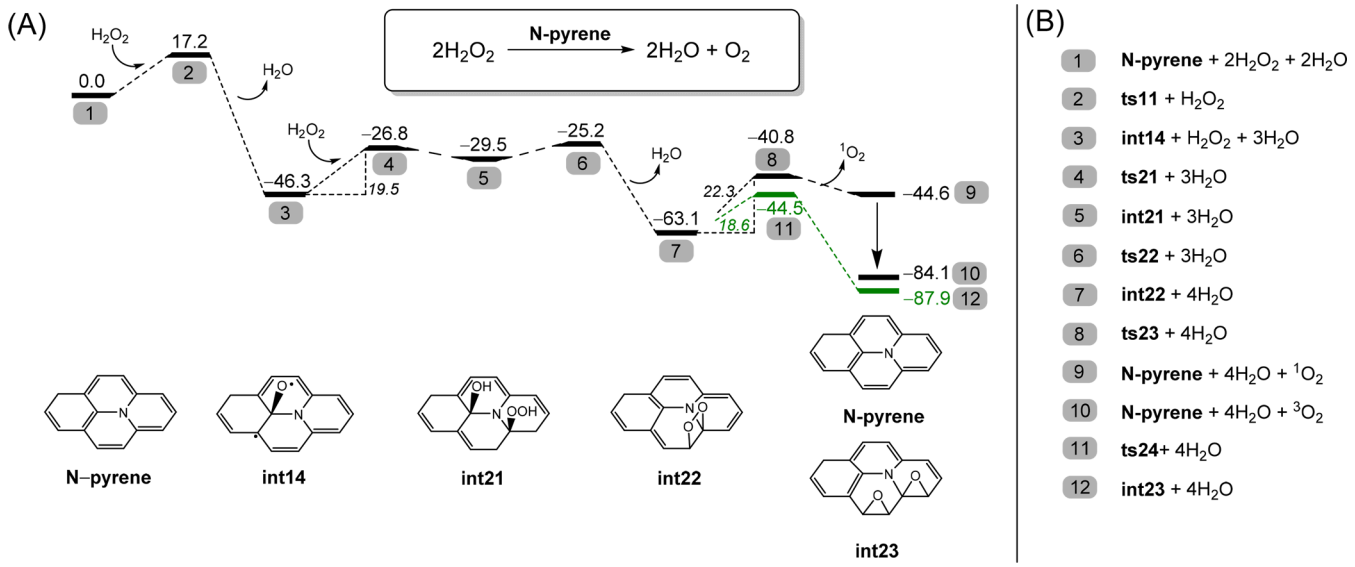

Figure 5. Calculated reaction energy profiles corresponding to the weak catalase-mimicking activity of N-pyrene, i.e., the small-sized model of N-rGO. (A) The black lines are the thermodynamically and kinetically less competitive catalytic cycle corresponding to the catalase-mimicking activity of N-pyrene through which two H_2O_2 molecules decompose to two H_2O and one O_2 molecules. The green lines represent the more competitive reaction channel yielding the diepoxy structure (energy in kcal/mol). (B) Chemical constituents for the stationary points shown in panel A.

activities of rGO and N-rGO-5 (Figure S14). Oxidase mimic was evaluated by monitoring the catalytic aerobic oxidation of TMB in the presence of rGO and N-rGO-5. As shown in Figure S14A, rGO exhibited negligible activity toward TMB oxidation, whereas N-rGO-5 showed slightly higher activity.

The SOD-mimicking activities were evaluated by monitoring the elimination of $^{\bullet}O_2^-$ by the nanozymes. As shown in Figure S14B, neither rGO nor N-rGO-5 could effectively eliminate $^{\bullet}O_2^-$, demonstrating the negligible SOD-like activity of the two nanomaterials.

Finally, the catalase-mimicking activities were evaluated by monitoring the production of O_2 from the nanozyme-catalyzed decomposition of H_2O_2. As shown in Figure S14C, the produced O_2 was measured with an air pressure detector. In the presence of rGO, the O_2 pressure was nearly the same as that observed without rGO. In the presence of N-rGO-5, the O_2 pressure slightly increased. These results demonstrated the very low catalase activities of rGO and N-rGO-5.

The normalized oxidase-, SOD-, and catalase-mimicking activities of rGO and N-rGO-5 are summarized in Figure 3A−3C. Further quantitative analysis showed that N-doping enhanced the peroxidase-mimicking activity of rGO by more than 100-fold. Unexpectedly, N-doping nearly showed negligible effects on the oxidase-, SOD-, and catalase-mimicking activities of rGO (Figure 3D). These results suggested that we had specifically enhanced the peroxidase-mimicking activity of rGO by doping N into rGO, which had not been achieved previously.

Mechanisms for Specifically Enhanced Peroxidase-Mimicking Activity of N-rGO. To reveal the reasons for the specific enhancement of the peroxidase-mimicking activity of rGO by N-doping, we performed DFT calculations to examine the possible catalytic reaction mechanisms responsible for the peroxidase, catalase-, oxidase-, and SOD-mimicking activities of N-rGO.

Figure 4 shows the reaction free energy profiles for the peroxidase-mimicking activity of N-pyrene (the smallest model of N-rGO, Figure S1). N-pyrene first captures an O atom from H_2O_2, generating an epoxy intermediate (**int11** of Figure 4A) and a molecule of water. Other water molecules can participate in this step, serving as the H-transfer catalysts to facilitate the reaction. Specifically, if two water molecules were involved as the H-transfer catalysts (in **ts11**), the corresponding Gibbs free energy of activation ($G‡$) was reduced to only 17.2 kcal/mol. Interestingly, the O atom of the epoxy group can freely move on the N-pyrene surface. The structural transformation from **int11** to **int14** (i.e., from 3 to 9 in Figure 4A), in which the O atom moves closer to the N atom, encounters successive energy barriers of only 3.6, 7.3, and 6.9 kcal/mol. Structure **int14** is a singlet diradical, whose unpaired electrons are located on the O atom and the adjacent C atom. Because of its high reactivity, the radical O of **int14** facilely abstracts an H atom from the peroxidase substrate TMB ($G‡$ = 12.2 kcal/mol), which generates **int15** and oxTMB (Figure 4A). Structure **int15** easily abstracts an H atom from another molecule of TMB ($G‡$ = 17.6 kcal/mol), which yields H_2O and another oxTMB, and simultaneously regenerates N-pyrene. The oxTMB can abstract a proton to form $oxTMBH^+$, which appears as blue in the experiment (Figure 4A). Through the catalytic cycle, two TMB molecules are oxidized by one molecule of H_2O_2 to generate two oxTMB and two H_2O molecules (Figure 4A, inset). The overall change in the Gibbs free energy (G_r) is −50.0 kcal/mol, and the largest $G‡$ is 17.6 kcal/mol. The negative G_r and low $G‡$ values mean that the N-pyrene-catalyzed oxidation of TMB by H_2O_2 is thermodynamically and kinetically favorable, which is in agreement with the experimentally observed high peroxidase-mimicking activity of N-rGO.

In the catalytic cycle shown in Figure 4A, the singlet diradical **int14** is the key reactive intermediate, whose radical O atom abstracts an H atom from TMB to produce the peroxidase-mimicking activity of N-pyrene. In the catalytic cycle, the structure **int12** is also a singlet diradical, which should also drive the peroxidase-mimicking activity for N-pyrene. In contrast, we failed to locate similar singlet diradical structures in the pyrene structure without N-doping. Instead,

DOI: 10.1021/acs.chemmater.8b02726
Chem. Mater. 2018, 30, 6431−6439

the O atoms on pyrene only formed epoxide structures. Therefore, the prominent peroxidase-mimicking activity of N-pyrene compared to that of pyrene was due to the N atoms of the former, which capture O atoms from H_2O_2 to form O-centered radicals. The radical O atoms then oxidize organic substrates. The above mechanism of peroxidase-mimicking activity of N-pyrene is consistent with the well-known catalytic mechanism of peroxidases: the iron porphyrin (i.e., the active site) takes an O atom from H_2O_2 to form the oxoiron(IV) porphyrin π-cation radical to further oxidize substrates.[55] These results are also in line with the mechanisms of the peroxidase- and oxidase-mimicking activities of metals, studies of which show that the O adatoms on metal surfaces are responsible for the oxidation of substrates.[29,34]

The calculations also revealed the prominent peroxidase-like activities for N-coronene (the larger cluster model of N-rGO) and N-graphene (the size-infinite model of N-rGO) (Figures S15A and S16). Therefore, computations with both the small-sized (N-pyrene and N-coronene) and size-infinite (N-graphene) models of N-rGO consistently verify the experimentally observed peroxidase-mimicking activity of N-rGO.

To explain the reasons for the negligible catalase-mimicking activity of N-rGO, we studied the reaction pathways corresponding to catalase-mimicking activity for N-pyrene, N-coronene, and N-graphene. The black lines in Figure 5A are the reaction free energy profiles for N-pyrene. First, N-pyrene is oxidized to **int14** following the same mechanism in Figure 4A. Then, **int21** forms through the dissociative addition of H_2O_2 to **int14**, which has an energy barrier of 19.5 kcal/mol. After a molecule of H_2O leaves **int21**, the endoperoxide structure **int22** is generated; this step is notably facile (G_r = −33.6 kcal/mol and $G‡$ = 4.3 kcal/mol). In principle, **int22** can be restored to N-pyrene by releasing a molecule of singlet oxygen ($^1O_2$). However, the $^1O_2$ releasing step is uncompetitive because of its relatively high energy barrier and positive change in the free energy ($G‡$ = 22.3 kcal/mol; G_r = 18.5 kcal/mol). Instead, the endoperoxide structure **int22** favors the O−O bond splitting reaction to form the diepoxy structure **int23** (Figure 5A, green; $G‡$ = 18.5 kcal/mol; G_r = −24.8 kcal/mol), which outcompetes the $^1O_2$ generation channel. Even considering that triplet oxygen $^3O_2$ can be formed through potential energy surface crossing (Figure S14), the $^3O_2$ releasing channel is still less competitive than the O−O splitting, leading to the diepoxy structure **int23**. Therefore, the catalase-mimicking activity of N-pyrene is low. Reportedly, endoperoxides can exist on GO and rGO[56] with high chemical reactivity.[57] Here, we show that the endoperoxide **int22** can easily transform into the diepoxy structure **int23**. As mentioned above, the epoxy O atom in the vicinity of graphitic N can be further converted to a radical O with high oxidizing capability, which instead agrees with peroxidase-mimicking activity. The reaction free energy profiles corresponding to catalase-mimicking activities of N-coronene and N-graphene are shown in Figures S15B and S18, respectively, which similarly predict minimal catalase-mimicking activities for N-rGO and agree with the experiment.

To explain the reasons for the weak SOD- and oxidase-mimicking activities of N-rGO, we calculated the corresponding reaction pathways with N-pyrene. We first studied whether N-pyrene can catalyze the disproportionation reaction of $^{\bullet}OOH$ to form H_2O_2 and O_2 as an SOD mimic. We used the $^{\bullet}OOH$ radical to represent $^{\bullet}O_2^-$ because of the known protonation reaction of $^{\bullet}O_2^-$ to form $^{\bullet}OOH$ under acidic conditions. Figure 6A shows the reaction energy profile corresponding to the SOD-mimicking reactions of N-pyrene.

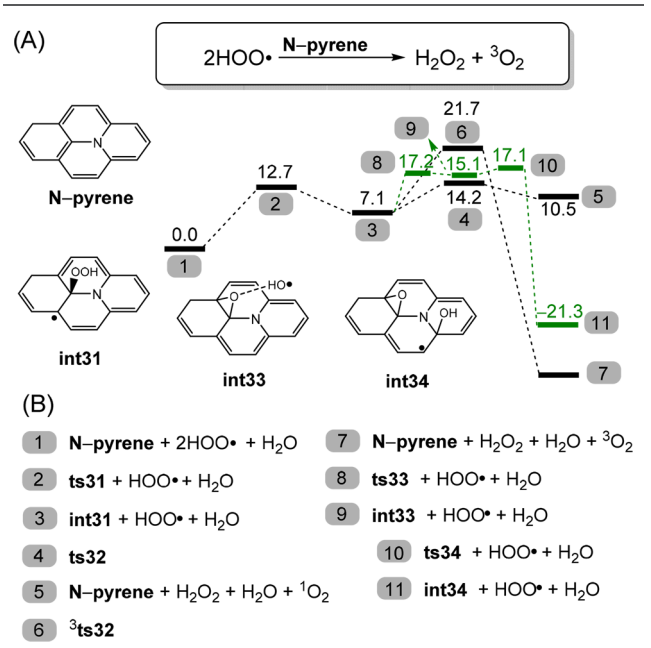

Figure 6. Calculated reaction free energy profiles corresponding to the weak SOD-mimicking activity of N-pyrene, i.e., the small-sized model of N-rGO. (A) The black lines are the less competitive catalytic cycle corresponding to the SOD-mimicking activity of N-pyrene through which two $^{\bullet}OOH$ radicals decompose to one H_2O_2 and one O_2 molecules. The green lines represent the more competitive reaction channel yielding the epoxy and hydroxyl structures (energy in kcal/mol). (B) Chemical constituents for the stationary points shown in panel A.

First, the radical $^{\bullet}OOH$ readily absorbs on the surface of N-pyrene to form intermediate **int31** (3 in Figure 6A), with an energy barrier of 12.7 kcal/mol. In principle, **int31** can react with another $^{\bullet}OOH$ to form one molecule of singlet $^1O_2$ and H_2O_2 (5 in Figure 6A), which is, however, thermodynamically unfavorable with the overall change in Gibbs free energy G_r of 10.5 kcal/mol. The reaction of **int31** with another $^{\bullet}OOH$ to form one molecule of triplet $^3O_2$ and H_2O_2 (7 in Figure 6A) is thermodynamically favorable, which, however, has a relatively higher energy barrier of 14.6 kcal/mol. Alternatively, the unimolecular transformation of **int31** to **int34** (i.e., an epoxide and a hydroxyl, 11 in Figure 6A) is thermodynamically favorable and has an energy barrier of only 10.1 kcal/mol. Importantly, this unimolecular transformation does not resort to the effective collision probability of **int34** with another $^{\bullet}OOH$ radical as the formation of $^1O_2$ or $^3O_2$ does, and thus would be more facile. The more facile transformation of $^{\bullet}OOH$ radicals to epoxy and hydroxyl groups instead of O_2 and H_2O_2 agrees with the weak SOD-mimicking activity of N-rGO observed in the experiment. The above data also rationalizes the weak oxidase-mimicking activity of N-rGO. As shown in Figure S17, the adsorption of $^3O_2$ to N-pyrene to form the endoperoxide structure **int22** is thermodynamically unfavorable with a high energy barrier, supporting the weak ability of N-rGO to activate $^3O_2$ and thus the inability of N-rGO to mimic oxidases.

Figure 7 summarizes the DFT results that account for the specific enhancement of peroxidase-mimicking activity of rGO

DOI: 10.1021/acs.chemmater.8b02726
Chem. Mater. 2018, 30, 6431−6439

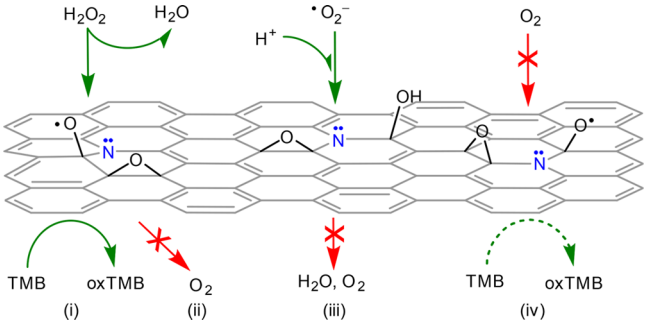

Figure 7. Mechanisms obtained by DFT calculations responsible for the specific peroxidase-mimicking activity (i) but negligible catalase-, SOD-, and oxidase-mimicking activities (ii, iii, and iv, respectively) of N-rGO.

by N-doping. The strong peroxidase-mimicking activity of N-rGO originates from the easy formation of radical oxygen species near the N sites of N-rGO from H_2O_2. Such radical oxygen species can be detached from the N-rGO surface after reacting with peroxidase substrates, rendering N-rGO peroxidase-mimicking activity. However, such radical oxygen species will form ring-closure epoxy species, which are difficult to be detached without the doping of nitrogen in rGO. So, N-doping, which probably stabilizes the radical oxygen species by nitrogen's lone pair electrons, is critical to enhance the peroxidase-mimicking activity of N-rGO. However, the recombination of the two oxygen adatoms into one molecule of free O_2 on N-rGO is less competitive than their transformation into two epoxy structures because of the strong chemisorption of O_2 on N-rGO. These results rationalize the weak catalase-mimicking activity of N-rGO. The strong chemisorption of O_2 on N-rGO also prevents the SOD-mimicking activity of N-rGO. In contrast, the reaction of $^{\bullet}O_2^-$ with N-rGO yields epoxy and hydroxyl species instead of O_2 and H_2O_2, in agreement with the weak SOD-mimicking activity of N-rGO. The large energy barrier for the chemisorption of $^3O_2$ on N-rGO, which arises from the spin conservation of $^3O_2$ when reacting with closed shell molecules, accounts for the weak oxidase-mimicking activity of N-rGO.

N-Doping as a General Strategy for Designing Highly Active and Specific Peroxidase-Mimicking Nanozymes. To test whether the N-doping strategy could also be used to engineer other carbon nanomaterials into highly active and specific peroxidase mimics, we doped MC with N and investigated the four enzyme-mimicking activities. Interestingly, N-MC also exhibits a much higher peroxidase-mimicking activity than MC (Figure S21). The quantitative analysis showed that the peroxidase-mimicking activity of MC was enhanced by more than 60-fold after N-doping. Moreover, both MC and N-MC exhibited nearly negligible oxidase-, SOD-, and catalase-mimicking activities (Figures 8B–8E). These results clearly demonstrated that N-MC also exhibits specifically enhanced peroxidase-like activity, indicating the generality of the N-doping strategy.

CONCLUSIONS

In summary, we demonstrated that the doping of heteroatom N into rGO and MC not only boosts their peroxidase-mimicking activities remarkably but also achieves exceptional specificity toward peroxidase-mimicking activity and no other closely related enzymatic reactions. The DFT calculations revealed the origin of such a high specificity, originating from the selective activation of H_2O_2 rather than O_2 and $^{\bullet}O_2^-$ by

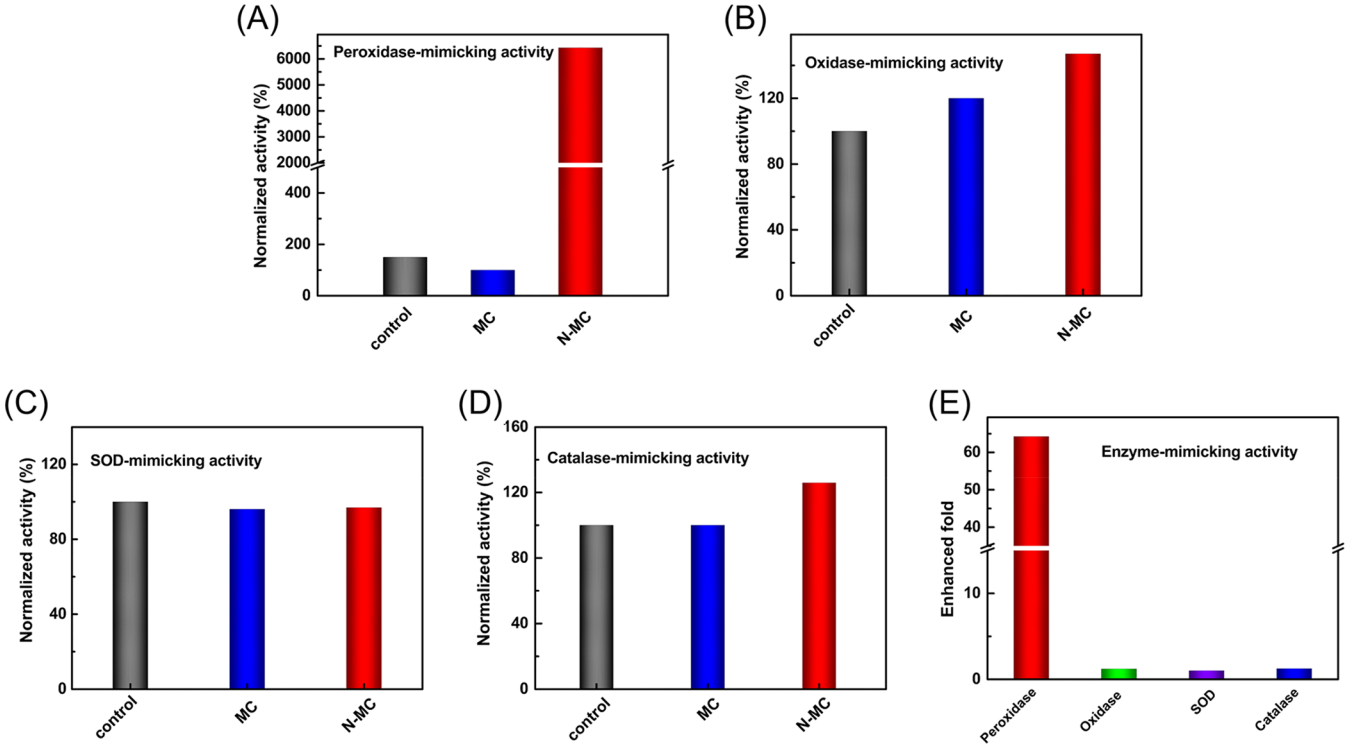

Figure 8. Specifically enhancing the peroxidase-mimicking activity of MC by N-doping. (A–D) Normalized peroxidase-, oxidase-, SOD-, and catalase-mimicking activities of MC and N-MC. Control was in the absence of nanozymes. (E) Enhancement of the enzyme-mimicking activities of N-MC relative to those of MC.

DOI: 10.1021/acs.chemmater.8b02726
Chem. Mater. 2018, 30, 6431–6439

the N-rGO. The N-rGO with specific peroxidase-like activities would show better sensing performance since it inhibited the decomposition of H_2O_2. Compared with rGO, N-rGO indeed showed wider linear range and lower detection limit for sensing of H_2O_2 (Figure S22). The current study not only demonstrates a new strategy to design highly active and specific peroxidase mimics but also provides deep insight into the catalytic mechanisms of these nanozymes. Given that carbon nanomaterials can be engineered by doping (and codoping) with other heteroatoms (such as P and S), it is anticipated that peroxidase-mimicking nanozymes with even higher catalytic activities will be developed in the future.

■ ASSOCIATED CONTENT

Supporting Information

The Supporting Information is available free of charge on the ACS Publications website at DOI: 10.1021/acs.chemmater.8b02726.

Extra figures with associated discussion; tables (PDF)

■ AUTHOR INFORMATION

Corresponding Authors

*E-mail: weihui@nju.edu.cn. Web: weilab.nju.edu.cn. Fax: +86-25-83594648. Tel.: +86-25-83593272.
*E-mail: gaox@jxnu.edu.cn.

ORCID

Zhong Jin: 0000-0001-8860-8579
Xingfa Gao: 0000-0002-1636-6336
Hui Wei: 0000-0003-0870-7142

Author Contributions

All authors have given approval to the final version of the manuscript.

Author Contributions

#These authors contributed equally.

Funding

This work was supported by National Natural Science Foundation of China (21874067, 21722503, and 21773095), 973 Program (2015CB659400), PAPD program, Shuangchuang Program of Jiangsu Province, Open Funds of the State Key Laboratory of Analytical Chemistry for Life Science (SKLACLS1704), Open Funds of the State Key Laboratory of Coordination Chemistry (SKLCC1819), China Postdoctoral Science Foundation (2018M630643), and Thousand Talents Program for Young Researchers.

Notes

The authors declare no competing financial interest.

■ ACKNOWLEDGMENTS

We thank Prof. Jin Xie, Prof. Wen Yang, and Yimeng Lian for help with carbon nanomaterials synthesis.

■ REFERENCES

(1) Wei, H.; Wang, E. K. Nanomaterials with Enzyme-Like Characteristics (Nanozymes): Next-Generation Aartificial Enzymes. *Chem. Soc. Rev.* **2013**, *42*, 6060−6093.

(2) Gao, L. Z.; Zhuang, J.; Nie, L.; Zhang, J. B.; Zhang, Y.; Gu, N.; Wang, T. H.; Feng, J.; Yang, D. L.; Perrett, S.; Yan, X. Intrinsic Peroxidase-Like Activity of Ferromagnetic Nanoparticles. *Nat. Nanotechnol.* **2007**, *2*, 577−583.

(3) Zhang, Z. J.; Zhang, X. H.; Liu, B. W.; Liu, J. W. Molecular Imprinting on Inorganic Nanozymes for Hundred-Fold Enzyme Specificity. *J. Am. Chem. Soc.* **2017**, *139*, 5412−5419.

(4) Liu, B. W.; Sun, Z. Y.; Huang, P. J. J.; Liu, J. W. Hydrogen Peroxide Displacing DNA from Nanoceria: Mechanism and Detection of Glucose in Serum. *J. Am. Chem. Soc.* **2015**, *137*, 1290−1295.

(5) Guo, Y. J.; Deng, L.; Li, J.; Guo, S. J.; Wang, E. K.; Dong, S. J. Hemin-Graphene Hybrid Nanosheets with Intrinsic Peroxidase-like Activity for Label-free Colorimetric Detection of Single-Nucleotide Polymorphism. *ACS Nano* **2011**, *5*, 1282−1290.

(6) Hu, Y. H.; Cheng, H. J.; Zhao, X. Z.; Wu, J. J.; Muhammad, F.; Lin, S. C.; He, J.; Zhou, L. Q.; Zhang, C. P.; Deng, Y.; Wang, P.; Zhou, Z. Y.; Nie, S. M.; Wei, H. Surface-Enhanced Raman Scattering Active Gold Nanoparticles with Enzyme-Mimicking Activities for Measuring Glucose and Lactate in Living Tissues. *ACS Nano* **2017**, *11*, 5558−5566.

(7) Wang, Q. Q.; Zhang, X. P.; Huang, L.; Zhang, Z. Q.; Dong, S. J. GOx@ZIF-8(NiPd) Nanoflower: An Artificial Enzyme System for Tandem Catalysis. *Angew. Chem., Int. Ed.* **2017**, *56*, 16082−16085.

(8) Gao, L.; Liu, M.; Ma, G.; Wang, Y.; Zhao, L.; Yuan, Q.; Gao, F.; Liu, R.; Zhai, J.; Chai, Z.; Zhao, Y.; Gao, X. Peptide-Conjugated Gold Nanoprobe: Intrinsic Nanozyme-Linked Immunsorbant Assay of Integrin Expression Level on Cell Membrane. *ACS Nano* **2015**, *9*, 10979−10990.

(9) Li, Y. Y.; He, X.; Yin, J. J.; Ma, Y. H.; Zhang, P.; Li, J. Y.; Ding, Y. Y.; Zhang, J.; Zhao, Y. L.; Chai, Z. F.; Zhang, Z. Y. Acquired Superoxide-Scavenging Ability of Ceria Nanoparticles. *Angew. Chem., Int. Ed.* **2015**, *54*, 1832−1835.

(10) Cai, R.; Yang, D.; Peng, S. J.; Chen, X. G.; Huang, Y.; Liu, Y.; Hou, W. J.; Yang, S. Y.; Liu, Z. B.; Tan, W. H. Single Nanoparticle to 3D Supercage: Framing for an Artificial Enzyme System. *J. Am. Chem. Soc.* **2015**, *137*, 13957−13963.

(11) Liu, Y.; Purich, D. L.; Wu, C.; Wu, Y.; Chen, T.; Cui, C.; Zhang, L.; Cansiz, S.; Hou, W.; Wang, Y.; Yang, S.; Tan, W. Ionic Functionalization of Hydrophobic Colloidal Nanoparticles To Form Ionic Nanoparticles with Enzymelike Properties. *J. Am. Chem. Soc.* **2015**, *137*, 14952−14958.

(12) Tonga, G. Y.; Jeong, Y. D.; Duncan, B.; Mizuhara, T.; Mout, R.; Das, R.; Kim, S. T.; Yeh, Y. C.; Yan, B.; Hou, S.; Rotello, V. M. Supramolecular Regulation of Bioorthogonal Catalysis in Cells Using Nanoparticle-Embedded Transition Metal Catalysts. *Nat. Chem.* **2015**, *7*, 597−603.

(13) Gupta, A.; Das, R.; Tonga, G. Y.; Mizuhara, T.; Rotello, V. M. Charge-Switchable Nanozymes for Bioorthogonal Imaging of Biofilm-Associated Infections. *ACS Nano* **2018**, *12*, 89−94.

(14) Manea, F.; Houillon, F. B.; Pasquato, L.; Scrimin, P. Nanozymes: Gold-Nanoparticle-Based Transphosphorylation Catalysts. *Angew. Chem., Int. Ed.* **2004**, *43*, 6165−6169.

(15) Chen, J.; Patil, S.; Seal, S.; McGinnis, J. F. Rare Earth Nanoparticles Prevent Retinal Degeneration Induced by Intracellular Peroxides. *Nat. Nanotechnol.* **2006**, *1*, 142−150.

(16) Fan, K. L.; Cao, C. Q.; Pan, Y. X.; Lu, D.; Yang, D. L.; Feng, J.; Song, L. N.; Liang, M. M.; Yan, X. Y. Magnetoferritin Nanoparticles for Targeting and Visualizing tumour tissues. *Nat. Nanotechnol.* **2012**, *7*, 459−464.

(17) Natalio, F.; Andre, R.; Hartog, A. F.; Stoll, B.; Jochum, K. P.; Wever, R.; Tremel, W. Vanadium Pentoxide Nanoparticles Mimic Vanadium Haloperoxidases and Thwart Biofilm Formation. *Nat. Nanotechnol.* **2012**, *7*, 530−535.

(18) Song, Y. J.; Qu, K. G.; Zhao, C.; Ren, J. S.; Qu, X. G. Graphene Oxide: Intrinsic Peroxidase Catalytic Activity and Its Application to Glucose Detection. *Adv. Mater.* **2010**, *22*, 2206−2210.

(19) Sun, H. J.; Zhao, A. D.; Gao, N.; Li, K.; Ren, J. S.; Qu, X. G. Deciphering a Nanocarbon-Based Artificial Peroxidase: Chemical Identification of the Catalytically Active and Substrate-Binding Sites on Graphene Quantum Dots. *Angew. Chem., Int. Ed.* **2015**, *54*, 7176−7180.

DOI: 10.1021/acs.chemmater.8b02726
Chem. Mater. 2018, 30, 6431−6439

(20) Ghosh, S.; Roy, P.; Karmodak, N.; Jemmis, E. D.; Mugesh, G. Nanoisozymes: Crystal-Facet-Dependent Enzyme-Mimetic Activity of V_2O_5 Nanomaterials. *Angew. Chem., Int. Ed.* **2018**, *57*, 4510−4515.
(21) Soh, M.; Kang, D. W.; Jeong, H. G.; Kim, D.; Kim, D. Y.; Yang, W.; Song, C.; Baik, S.; Choi, I. Y.; Ki, S. K.; Kwon, H. J.; Kim, T.; Kim, C. K.; Lee, S. H.; Hyeon, T. Ceria-Zirconia Nanoparticles as an Enhanced Multi-Antioxidant for Sepsis Treatment. *Angew. Chem., Int. Ed.* **2017**, *56*, 11399−11403.
(22) Zaramella, D.; Scrimin, P.; Prins, L. J. Self-Assembly of a Catalytic Multivalent Peptide-Nanoparticle Complex. *J. Am. Chem. Soc.* **2012**, *134*, 8396−8399.
(23) Kim, M.; Kim, M. S.; Kweon, S. H.; Jeong, S.; Kang, M. H.; Kim, M. I.; Lee, J.; Doh, J. Simple and Sensitive Point-of-Care Bioassay System Based on Hierarchically Structured Enzyme-Mimetic Nanoparticles. *Adv. Healthcare Mater.* **2015**, *4*, 1311−1316.
(24) Cheng, H.; Liu, Y.; Hu, Y.; Ding, Y.; Lin, S.; Cao, W.; Wang, Q.; Wu, J.; Muhammad, F.; Zhao, X.; Zhao, D.; Li, Z.; Xing, H.; Wei, H. Monitoring of Heparin Activity in Live Rats Using Metal-Organic Framework Nanosheets as Peroxidase Mimics. *Anal. Chem.* **2017**, *89*, 11552−11559.
(25) Fang, G.; Li, W.; Shen, X.; Perez-Aguilar, J. M.; Chong, Y.; Gao, X.; Chai, Z.; Chen, C.; Ge, C.; Zhou, R. Differential Pd-Nanocrystal Facets Demonstrate Distinct Antibacterial Activity Against Gram-Positive and Gram-Negative Bacteria. *Nat. Commun.* **2018**, *9*, 129.
(26) Karakoti, A.; Singh, S.; Dowding, J. M.; Seal, S.; Self, W. T. Redox-Active radical Scavenging Nanomaterials. *Chem. Soc. Rev.* **2010**, *39*, 4422−4432.
(27) Lu, C. H.; Yang, H. H.; Zhu, C. L.; Chen, X.; Chen, G. N. A Graphene Platform for Sensing Biomolecules. *Angew. Chem.* **2009**, *121*, 4879−4881.
(28) Fan, K. L.; Wang, H.; Xi, J. Q.; Liu, Q.; Meng, X. Q.; Duan, D. M.; Gao, L. Z.; Yan, X. Y. Optimization of Fe_3O_4 Nanozyme Activity via Single Amino Acid Modification Mimicking an Enzyme Active Site. *Chem. Commun.* **2017**, *53*, 424−427.
(29) Shen, X.; Liu, W.; Gao, X.; Lu, Z.; Wu, X.; Gao, X. Mechanisms of Oxidase and Superoxide Dismutation-like Activities of Gold, Silver, Platinum, and Palladium, and Their Alloys: A General Way to the Activation of Molecular Oxygen. *J. Am. Chem. Soc.* **2015**, *137*, 15882−15891.
(30) Asati, A.; Santra, S.; Kaittanis, C.; Nath, S.; Perez, J. M. Oxidase-Like Activity of Polymer-Coated Cerium Oxide Nanoparticles. *Angew. Chem., Int. Ed.* **2009**, *48*, 2308−2312.
(31) Lin, L.; Song, X.; Chen, Y.; Rong, M.; Zhao, T.; Wang, Y.; Jiang, Y.; Chen, X. Intrinsic Peroxidase-Like Catalytic Activity of Nitrogen-Doped Graphene Quantum Dots and Their Application in the Colorimetric Detection of H_2O_2 and Glucose. *Anal. Chim. Acta* **2015**, *869*, 89−95.
(32) Fan, K.; Xi, J.; Fan, L.; Wang, P.; Zhu, C.; Tang, Y.; Xu, X.; Liang, M.; Jiang, B.; Yan, X.; Gao, L. Vivo Guiding Nitrogen-Doped Carbon Nanozyme for Tumor Catalytic Therapy. *Nat. Commun.* **2018**, *9*, 1440−1450.
(33) Zhang, W.; Hu, S.; Yin, J.-J.; He, W.; Lu, W.; Ma, M.; Gu, N.; Zhang, Y. Prussian Blue Nanoparticles as Multienzyme Mimetics and Reactive Oxygen Species Scavengers. *J. Am. Chem. Soc.* **2016**, *138*, 5860−5865.
(34) Li, J. N.; Liu, W. Q.; Wu, X. C.; Gao, X. F. Mechanism of pH-Switchable Peroxidase and Catalase-Like Activities of Gold, Silver, Platinum and Palladium. *Biomaterials* **2015**, *48*, 37−44.
(35) Chen, Z.; Yin, J. J.; Zhou, Y. T.; Zhang, Y.; Song, L.; Song, M.; Hu, S.; Gu, N. Dual Enzyme-like Activities of Iron Oxide Nanoparticles and Their Implication for Diminishing Cytotoxicity. *ACS Nano* **2012**, *6*, 4001−4012.
(36) Dugan, L. L.; Turetsky, D. M.; Du, C.; Lobner, D.; Wheeler, M.; Almli, C. R.; Shen, C. K. F.; Luh, T. Y.; Choi, D. W.; Lin, T. S. Carboxyfullerenes As Neuroprotective Agents. *Proc. Natl. Acad. Sci. U. S. A.* **1997**, *94*, 9434−9439.
(37) Li, R.; Zhen, M.; Guan, M.; Chen, D.; Zhang, G.; Ge, J.; Gong, P.; Wang, C.; Shu, C. A novel Glucose Colorimetric Sensor Based on Intrinsic Peroxidase-Like Activity of C_{60}-Carboxyfullerenes. *Biosens. Bioelectron.* **2013**, *47*, 502−507.
(38) Shi, W.; Wang, Q.; Long, Y.; Cheng, Z.; Chen, S.; Zheng, H.; Huang, Y. Carbon Nanodots As Peroxidase Mimetics and Their Applications to Glucose Detection. *Chem. Commun.* **2011**, *47*, 6695−6697.
(39) Samuel, E. L. G.; Marcano, D. C.; Berka, V.; Bitner, B. R.; Wu, G.; Potter, A.; Fabian, R. H.; Pautler, R. G.; Kent, T. A.; Tsai, A. L.; Tour, J. M. Highly Efficient Conversion of Superoxide to Oxygen Using Hydrophilic Carbon Clusters. *Proc. Natl. Acad. Sci. U. S. A.* **2015**, *112*, 2343−2348.
(40) Jin, J.; Fu, X.; Liu, Q.; Liu, Y.; Wei, Z.; Niu, K.; Zhang, J. Identifying the Active Site in Nitrogen-Doped Graphene for the VO^{2+}/VO_2^+ Redox Reaction. *ACS Nano* **2013**, *7*, 4764−4773.
(41) Lai, L.; Potts, J. R.; Zhan, D.; Wang, L.; Poh, C. K.; Tang, C.; Gong, H.; Shen, Z.; Lin, J.; Ruoff, R. S. Exploration of the Active Center Structure of Nitrnogen-Doped Graphene-Based Catalysts for Oxygen Reduction Reaction. *Energy Environ. Sci.* **2012**, *5*, 7936−7942.
(42) Muhammad, F.; Guo, M.; Qi, W.; Sun, F.; Wang, A.; Guo, Y.; Zhu, G. pH-Triggered Controlled Drug Release from Mesoporous Silica Nanoparticles via Intracelluar Dissolution of ZnO Nanolids. *J. Am. Chem. Soc.* **2011**, *133*, 8778−8781.
(43) Liang, C.; Li, Z.; Dai, S. Mesoporous Carbon Materials: Synthesis and Modification. *Angew. Chem., Int. Ed.* **2008**, *47*, 3696−3717.
(44) Lu, A. H.; Li, W. C.; Schmidt, W.; Kiefer, W.; Schüth, F. Easy Synthesis of an Ordered Mesoporous Carbon with a Hexagonally Packed Tubular Structure. *Carbon* **2004**, *42*, 2939−2948.
(45) Li, X.-F.; Lian, K.-Y.; Liu, L.; Wu, Y.; Qiu, Q.; Jiang, J.; Deng, M.; Luo, Y. Unraveling the Formation Mechanism of Graphitic Nitrogen-Doping in Thermally Treated Graphene with Ammonia. *Sci. Rep.* **2016**, *6*, 23495.
(46) Sharifi, T.; Hu, G.; Jia, X.; Wagberg, T. Formation of Active Sites for Oxygen Reduction Reactions by Transformation of Nitrogen Functionalities in Nitrogen-Doped Carbon Nanotubes. *ACS Nano* **2012**, *6*, 8904−8912.
(47) He, W.; Jiang, C.; Wang, J.; Lu, L. High-Rate Oxygen Electroreduction Over Graphitic-N Species Exposed on 3D Hierarchically Porous Nitrogen-Doped Carbons. *Angew. Chem., Int. Ed.* **2014**, *53*, 9503−9507.
(48) Zhao, R. S.; Zhao, X.; Gao, X. F. Molecular-Level Insights into Intrinsic Peroxidase-Like Activity of Nanocarbon Oxides. *Chem. - Eur. J.* **2015**, *21*, 960−964.
(49) Cohen, A. J.; Handy, N. C. Dynamic Correlation. *Mol. Phys.* **2001**, *99*, 607−615.
(50) Tomasi, J.; Mennucci, B.; Cammi, R. Quantum Mechanical Continuum Solvation Models. *Chem. Rev.* **2005**, *105*, 2999−3094.
(51) Frisch, M. J.; Trucks, G. W.; Schlegel, H. B.; Scuseria, G. E.; Robb, M. A.; Cheeseman, J. R.; Scalmani, G.; Barone, V.; Mennucci, B.; Petersson, G. A. *Gaussian 09*, revision A.02; Gaussian, Inc.:Wallingford, CT, 2009.
(52) Kresse, G.; Furthmuller, J. Efficient Iterative Schemes for Ab Initio Total-Energy Calculations Using a Plane-Wave BasisSet. *Phys. Rev. B: Condens. Matter Mater. Phys.* **1996**, *54*, 11169−11186.
(53) Perdew, J. P.; Burke, K.; Ernzerhof, M. Generalized gradient approximation made simple. *Phys. Rev. Lett.* **1996**, *77*, 3865−3868.
(54) Monkhorst, H. J.; Pack, J. D. Special Points for Brillouin-Zone Tntegrations. *Phys. Rev. B* **1976**, *13*, 5188−5192.
(55) Fasan, R. New Functional Twists for P450s. *Nat. Chem.* **2017**, *9*, 609−611.
(56) Vernekar, A. A.; Mugesh, G. Catalytic Reduction of Graphene Oxide Nanosheets by Glutathione Peroxidase Mimetics Reveals a New Structural Motif in Graphene Oxide. *Chem. - Eur. J.* **2013**, *19*, 16699−16706.
(57) Pieper, H.; Chercheja, S.; Eigler, S.; Halbig, C. E.; Filipovic, M. R.; Mokhir, A. Endoperoxides Revealed as Origin of the Toxicity of Graphene Oxide. *Angew. Chem., Int. Ed.* **2016**, *55*, 405−407.

DOI: 10.1021/acs.chemmater.8b02726
Chem. Mater. 2018, 30, 6431−6439